Journal of
Mechanics of
Materials and Structures

ANTIPLANE SHEAR FIELD FOR A CLASS OF HYPERELASTIC INCOMPRESSIBLE BRITTLE MATERIAL: ANALYTICAL AND NUMERICAL APPROACHES

Claude Stolz and Andres Parrilla Gomez

Volume 10, No. 3 May 2015

msp

JOURNAL OF MECHANICS OF MATERIALS AND STRUCTURES
Vol. 10, No. 3, 2015
dx.doi.org/10.2140/jomms.2015.10.395

msp

ANTIPLANE SHEAR FIELD FOR A CLASS OF HYPERELASTIC INCOMPRESSIBLE BRITTLE MATERIAL: ANALYTICAL AND NUMERICAL APPROACHES

CLAUDE STOLZ AND ANDRES PARRILLA GOMEZ

This paper reconsiders the problem of determining the elastostatics fields near the tip of a crack in a body deformed by an antiplane shear for a class of incompressible, homogeneous, isotropic materials. The study is generalized to the formation of a quasicrack under the same conditions of loading for brittle material that cannot support any further loading when a critical strength is reached. The crack is then replaced by a totally damaged zone where the stress is identically zero. The shape of the boundary between the damaged and undamaged body is found analytically. A numerical approach is proposed to address the problem for more general constitutive law. The analytical solution is recovered by a process of shape optimization.

1. Introduction

In classical fracture mechanics, the solution of equilibrium for linearized elastostatics proposes an outer expansion of the displacement with respect to the distance from the crack tip. Some studies have taken into account the nonlinear effects on the inner expansion of the displacement in finite elastostatics or in elastoplasticity. The finite antiplane shear near the tip of a crack in an incompressible nonlinear elastic solid has been studied [Knowles and Sternberg 1980; 1981]. The displacement field possesses singularities or discontinuities in its gradient depending on the shape of the stress-strain curve. For these studies, the stress is defined for any amount of shear that is not bounded.

For hyperelastic material such as elastomers, rupture may occur when a maximal stretch is reached. When this critical value is reached, the material is broken and cannot support further tension: then a damaged zone develops inside the body. The purpose of this paper is to determine the shape of the damaged zone under antiplane shear conditions.

Neuber [1968] investigated the mechanism of nonlinear stress-concentration near a notch and crack propagation. The solution is obtained for any nonlinear stress-strain laws monotonically increasing and all loading intensities. The boundary of the notch consists of two parallel straight lines and a cycloid along which the amount of shear is uniform. Bui and Ehrlacher [1980] solved the same problem for a linear elastic-brittle material; the thickness of the damaged zone is determined as a function of the stress intensity factor of the equivalent crack. A similar solution has been obtained for elastoplasticity [Bui 1980].

More recently, brittle hyperelastic material solution for constitutive laws that permit loss of ellipticity has been considered. Under antiplane shear, the boundary governed by the critical value of shear is a cycloid [Stolz 2010] using the hodograph scheme as proposed in [Knowles and Sternberg 1980].

These studies are supported by the ERC program.
Keywords: antiplane shear, brittle material, crack-tip fields, hyperelasticity.

Under the antiplane condition, during the propagation, the cracks tend to deviate from their plane. The purpose of this paper is not to study the propagation of the crack in a three-dimensional space. The antiplane problem is considered here to provide an analytical solution to evaluate the ability of the proposed numerical scheme to determine a stress-free boundary independently of the mesh of a body.

2. Preliminaries and finite antiplane shear

Consider an isotropic homogeneous incompressible elastic body. Suppose that the body occupies an open region Ω in a nondeformed configuration, and let us consider a deformation defined by the plane displacement $w(\boldsymbol{x})$,

$$\boldsymbol{y}(\boldsymbol{x}) = \boldsymbol{x} + w(x_1, x_2)\boldsymbol{e}_3, \tag{2-1}$$

that maps the domain Ω onto its deformation image ω. We assume that the mapping is regular and invertible. Let

$$\boldsymbol{F} = \boldsymbol{I} + w_{,i}\boldsymbol{e}_3 \otimes \boldsymbol{e}_i, \qquad \boldsymbol{F}^{-1} = \boldsymbol{I} - w_{,i}\boldsymbol{e}_3 \otimes \boldsymbol{e}_i, \tag{2-2}$$

the deformation gradient and its inverse. For an incompressible medium, the volume must be locally preserved and thus

$$J = \det \boldsymbol{F} = 1. \tag{2-3}$$

The left Cauchy–Green deformation tensor

$$\boldsymbol{B} = \boldsymbol{I} + w_{,i}(\boldsymbol{e}_3 \otimes \boldsymbol{e}_i + \boldsymbol{e}_i \otimes \boldsymbol{e}_3) + (w_{,x_1}^2 + w_{,x_2}^2)\boldsymbol{e}_3 \otimes \boldsymbol{e}_3 \tag{2-4}$$

has the fundamental scalar invariants

$$I_1 = \operatorname{Tr} \boldsymbol{B}, \qquad I_2 = \tfrac{1}{2}(I_1^2 - \operatorname{Tr}(\boldsymbol{B}^2)), \qquad I_3 = J^2 = 1. \tag{2-5}$$

The invariants I_1 and I_2 are equal:

$$I_1 = I_2 = 3 + R^2, \tag{2-6}$$

where R is the norm of ∇w.

For hyperelastic isotropic incompressible material, the free energy is a function E of these invariants; in the case of antiplane shear, this energy is reduced to a function Ψ:

$$\Psi(I_1) = E(I_1, I_2). \tag{2-7}$$

For the energy Ψ, the constitutive behavior is written as

$$\boldsymbol{\Theta} = 2\Psi'(I_1)\boldsymbol{F}^T + \eta \boldsymbol{F}^{-1}, \qquad \boldsymbol{\sigma} = 2\Psi'(I_1)\boldsymbol{B} + \eta \boldsymbol{I}, \tag{2-8}$$

where $\boldsymbol{\Theta}$ is the first Piola–Kirchhof stress tensor and $\boldsymbol{\sigma}$ the (actual) Cauchy stress tensor and where the Lagrange multiplier η is associated with the constraint (2-3).

The balance of linear momentum in the absence of body forces leads to the equilibrium equation

$$\operatorname{Div} \boldsymbol{\Theta}^T = 2(\Psi'(I_1)w_{,\beta})_{,\beta} = 0, \tag{2-9}$$

where $\beta = 1, 2$ and the summation is implied. This equation is that obtained in small perturbation for nonlinear elastic material with modulus $\mu = \Psi'(I_1)$.

As $\boldsymbol{\sigma} \cdot \boldsymbol{e}_3 = 0$, the associated Piola stress tensor $\boldsymbol{\Theta}$ is then reduced to

$$\boldsymbol{\Theta} = 2\Psi'(\boldsymbol{F}^T - \boldsymbol{F}^{-1}), \tag{2-10}$$

and the balance of linear momentum leads to an elliptic differential equation under the condition

$$2\Psi' + 4R^2\Psi'' \geq 0, \tag{2-11}$$

which corresponds to the fact that the local stress-strain curve $\tau(R) = 2R\Psi'(R) = R\mu(R)$ is an increasing function of R.

2A. ***Power law for $\alpha \leq 1$.*** Assume now that the local stress-strain relations are given by

$$\begin{cases} R \leq R_o, & \tau = \mu_o R, \\ R_o \leq R \leq R_m, & \tau = \mu_o R_o (R/R_o)^\alpha = \hat{\mu} R^\alpha, \\ R_m \leq R, & \tau = 0. \end{cases} \tag{2-12}$$

Then for $R \leq R_o$, the differential equation is elliptic. For $R_m \geq R \geq R_o$, ellipticity is ensured if $\alpha \geq 0$; otherwise, the differential equation becomes hyperbolic.

2B. ***Neo-Hookean material.*** For $\alpha = 1$ and $R_m = \infty$, the material is neo-Hookean. For this case, the differential equation reduces to Laplace's equation and for a straight crack ($-\infty \leq X_1 \leq 0$ and $X_2 = 0$) the solution of equilibrium is identical to the solution of Irwin obtained for linearized elastostatic. In the radial coordinates around the crack tip, the displacement is obtained as

$$w \to \frac{2K}{\mu_o}\sqrt{\frac{r}{2\pi}}\sin\frac{\theta}{2}, \quad r \to \infty. \tag{2-13}$$

3. The small-scale nonlinear quasicrack problem and hodograph transformation

To determine the mechanical fields over the domain Ω, the hodograph transformation is useful as pointed out by [Knowles and Sternberg 1980; 1981]. Other techniques can be used [Neuber 1968]. In the hodograph transformation, the components of the gradient ∇w become the new independent variables:

$$(x_1, x_2) \to (\xi_1, \xi_2), \quad \xi_\alpha = w_{,\alpha}(x_1, x_2). \tag{3-1}$$

The displacement appears as a potential ($dw = \xi_\alpha\, dx_\alpha$). The mapping is invertible provided the Jacobian $H = w_{,11}w_{,22} - (w_{,12})^2$ does not vanish. Denote by U the Legendre transformation of w with respect to ξ_α:

$$U(\xi_1, \xi_2) = x_\alpha w_{,\alpha}(x_1, x_2) - w(x_1, x_2). \tag{3-2}$$

By differentiating U with respect to ξ, the conjugate equations are obtained:

$$x_\alpha = \frac{\partial U}{\partial \xi_\alpha}, \qquad w = \xi \cdot \nabla U - U. \tag{3-3}$$

In the hodograph plane, the polar coordinates are used ($\xi_1 = R\cos\Theta$ and $\xi_2 = R\sin\Theta$); then this inverse of the mapping is given by

$$x_1 = \cos\Theta\frac{\partial U}{\partial R} - \frac{\sin\Theta}{R}\frac{\partial U}{\partial \Theta}, \qquad x_2 = \sin\Theta\frac{\partial U}{\partial R} + \frac{\cos\Theta}{R}\frac{\partial U}{\partial \Theta}. \tag{3-4}$$

The stress field satisfies

$$\tau_1 = \boldsymbol{\sigma}_{13} = \mu(R)R\cos\Theta, \qquad \tau_2 = \boldsymbol{\sigma}_{23} = \mu(R)R\sin\Theta. \tag{3-5}$$

The equation of motion (2-9) is rewritten in the hodograph plane (R, Θ) using the mapping (3-4). The notation $(\,\cdot\,)'$ indicates a differentiation with respect to R. The differential equation obtained in statics takes the expression

$$\frac{\partial}{\partial R}\left(\mu(R)R\frac{\partial U}{\partial R}\right) + \frac{(\mu(R)R)'}{R}\frac{\partial^2 U}{\partial \Theta^2} = 0. \tag{3-6}$$

This equation is homogeneous of degree 1 in U. Using (3-2), the displacement w is

$$w = R^2\frac{\partial}{\partial R}\frac{U}{R}. \tag{3-7}$$

3A. ***Crack in a neo-Hookean material.*** A solution of (3-6) for a given modulus $\mu(R)$ is

$$U(R, \Theta) = A_o R I_o(R)\cos\Theta, \quad R \geq 0,\ 0 \leq \Theta \leq \pi, \tag{3-8}$$

where the function $I_o(R)$ is

$$I_o(R) = \int_R^\infty \frac{\mathrm{d}t}{\mu(t)t^3}. \tag{3-9}$$

For neo-Hookean materials, the modulus $\mu(t)$ is a constant μ_o and the solution is then

$$U(R, \Theta) = \frac{A_o}{2\mu_o R}\cos\Theta, \qquad w = -\frac{A_o}{\mu_o R}\cos\Theta. \tag{3-10}$$

The images of the crack lips ($\theta = \pm\pi$) are the two ξ_1 axes $\Theta = 0$ and $\Theta = \pi$. The boundary conditions on the crack lips are

$$\frac{\partial U}{\partial \Theta} = 0 \quad \text{for all } R,\ \Theta = 0, \text{ and } \Theta = \pi. \tag{3-11}$$

Taking into account the hodograph transformation (3-4) and Irwin's solution (2-13), we obtain the identification

$$\Theta = \tfrac{1}{2}(\pi + \theta), \qquad A_o = \frac{K^2}{\pi\mu_o}. \tag{3-12}$$

3B. ***On the solution for power law for $R_m \to \infty$.*** It is easy to verify that the potential U_α given by

$$U_\alpha(R, \Theta) = A_\alpha R\cos\Theta\int_R^{R_o}\frac{\mathrm{d}t}{\hat{\mu}_o t^{\alpha+2}} = A_\alpha R I_\alpha(R)\cos\Theta \tag{3-13}$$

satisfies the conservation (2-9) of linear momentum for $\alpha \neq -1$.

For the proposed strain-stress law with $R_m \to \infty$, the solution U is obtained:

- on domain $R \leq R_o$, $\alpha = 1$ and $U = A_1 R I_1(R)\cos\Theta$ and
- on domain $R \geq R_o$, $U = A_\alpha R I_\alpha(R)\cos\Theta$.

The constant A_1 is determined by the condition of the loading at infinity (4-5). The potential at shear amount $R = R_o$ is continuous.

For $\alpha \geq 0$, the differential equation is elliptic for all amounts of shear, and the continuity of the displacement for $R = R_o$ for all Θ gives the constant A_α. On this curve, the stress is also continuous.

For $\alpha < 0$ and $R \geq R_o$, the differential equation is hyperbolic. In this case, the elliptic and hyperbolic domains are not disjoint. The potential is continuous for $R = R_o$ but not the displacement. The solution in the elliptic domain must be equal to the solution in the hyperbolic domain: $w_e(R_e, \Theta_e) = w_h(R_h, \Theta_h)$ at the common point $(x_1^e(R_e, \Theta_e) = x_1^h(R_h, \Theta_h), x_2^e(R_e, \Theta_e) = x_2^h(R_h, \Theta_h))$. These equations determine a curve where the gradient of the displacement is discontinuous [Knowles and Sternberg 1981] and the stress vector is continuous. The continuity of the stress vector implies that $A_\alpha = A_o$. The resulting potential is that of Knowles and Sternberg [1981].

3C. ***On the quasicrack geometry.*** To obtain the geometry of the quasicrack, other solutions of (2-9) must be added. Peculiar functions of the differential equation are

$$R\left(\frac{2\alpha}{\alpha+1}\log R\cos\Theta - \Theta\sin\Theta\right), \qquad R\cos\Theta, \qquad R\sin\Theta. \tag{3-14}$$

The first one corresponds to a shift along x_2 when Θ goes from 0 to π, the second permits an x_1 shift of a unit value, and the last one corresponds to a shift along $\boldsymbol{e}_2$ of a unit value.

4. The quasicrack solution

For the considered example, the geometry of the crack is the straight line $-\infty \leq x_1 \leq 0$. The direction of the line is $\boldsymbol{e}_1$. The applied loading is that of a crack obtained in classical linearized elasticity or embedded in neo-Hookean material as presented in Section 1. For an inner point of view, the local behavior is nonlinear and the amount of shear is limited by a critical value R_m as described by the proposed constitutive law.

For the considered constitutive law, the solution in the hodograph plane is built by the combination of the solution for the linear part of the constitutive law and the solution for the nonlinear part with the help of peculiar solutions.

Using the above results, the potential U is searched by

$$\begin{cases} 0 \leq R \leq R_o, & U = U_o(R,\Theta), \\ & U_o = A_o R\cos\Theta \displaystyle\int_R^{R_o} \frac{\mathrm{d}t}{\mu_o t^3} - B_o R(\log R\cos\Theta - \Theta\sin\Theta) + C_o R\cos\Theta, \\ R_o \leq R \leq R_m, & U_1 = \widehat{U}(R,\Theta), \\ & U_1 = A_1 R\cos\Theta \displaystyle\int_R^{R_o} \frac{\mathrm{d}t}{\hat{\mu}_o t^{\alpha+2}} - B_1 R\left(\frac{2\alpha}{\alpha+1}\log R\cos\Theta - \Theta\sin\Theta\right) + C_1 R\cos\Theta. \end{cases} \tag{4-1}$$

The constants $(A_o, A_1, B_o, B_1, C_o, C_1)$ are determined by

(a) continuity conditions of the potential in $R = R_o$,

(b) continuity of the displacement w everywhere,

(c) asymptotic behavior when $R \to 0$, and

(d) traction-free boundary conditions along the boundary of the damaged zone.

4A. ***Determination of the constants.***

(a) The continuity of the potential implies that $B_o = B_1 = B$ and the relation

$$B\frac{2\alpha}{\alpha+1}R_o\log R_o + C_1 R_o = BR_o\log R_o + C_o R_o. \tag{4-2}$$

Then the displacement is given by

$$\begin{cases} 0 \le R \le R_o, & w = w_o(R,\Theta) = -\left(\dfrac{A_o}{\mu_o R} + BR\right)\cos\Theta, \\ R_o \le R \le R_m, & w = \hat{w}(R,\Theta) = -\left(\dfrac{A_1}{\hat{\mu}_o R^\alpha} + \dfrac{2B\alpha}{\alpha+1}R\right)\cos\Theta. \end{cases} \tag{4-3}$$

(b) The displacement is continuous on $R = R_o$:

$$A_1 + \mu_o R_o^2 B\frac{\alpha-1}{\alpha+1} = A_o. \tag{4-4}$$

(c) The displacement satisfies the matching condition at ∞, so we obtain

$$A_o = \frac{K^2}{\pi\mu_o}. \tag{4-5}$$

(d) The boundary along the damaged zone is traction-free.

To simplify the expression, we adopt an dimensionless formulation. Let us define new parameters (a, a_1, b)

$$\frac{A_o}{\mu_o R_o^2} = \frac{K^2}{\pi\tau_o^2} = a, \qquad \frac{A_1}{\mu_o R_o^2} = aa_1, \qquad B = ba. \tag{4-6}$$

We adopt $C_o = 2 - B + B\log R_o$ in order to determine the position of the quasicrack along $x_2 = 0$, and we consider the notation $X_i = x_i/a$ and $\rho = R/R_o$. Then $\rho_o = 1$ and $\rho_m = R_m/R_o$.

The condition (4-5) is then rewritten as

$$a_1 + b\frac{\alpha-1}{\alpha+1} = 1. \tag{4-7}$$

With this notation, the traction-free boundary condition (d) is now explained.

For that, the image of the hodograph plane is determined:

- $0 \le \rho \le 1$,

$$X_1 = -\frac{1}{2} - \frac{1}{2\rho^2}\cos 2\Theta - b\log\rho,$$
$$X_2 = -\frac{1}{2\rho^2}\sin 2\Theta + b\left(\Theta - \frac{\pi}{2}\right),$$
$$W = -\left(\frac{1}{\rho} + b\rho\right)\cos\Theta,$$

- $1 \le \rho \le \rho_m$,

$$X_1 = -\left(\frac{a_1}{\rho^{\alpha+1}} + b\frac{\alpha-1}{\alpha+1}\right)\frac{\cos 2\Theta}{2} - \left(\frac{a_1}{\rho^{\alpha+1}} + b\right)\frac{\alpha-1}{2(\alpha+1)} - \frac{2b\alpha}{\alpha+1}\log\rho - \frac{a_1}{\alpha+1},$$
$$X_2 = -\left(\frac{a_1}{\rho^{\alpha+1}} + b\frac{\alpha-1}{\alpha+1}\right)\frac{\sin 2\Theta}{2} + b\left(\Theta - \frac{\pi}{2}\right),$$
$$W = -\left(\frac{a_1}{\rho^{\alpha}} + \frac{2\alpha}{\alpha+1}b\rho\right)\cos\Theta.$$

We have moved the frame along $\boldsymbol{e}_2$ with a shift of $-b\pi/2$ to emphasize the symmetry of the geometry with respect to $\boldsymbol{e}_1$. For $\rho = \rho_a$, the curve $(X_1(\rho_a, \Theta), X_2(\rho_a, \Theta))$ is a cycloid. With this geometry, the traction-free boundary condition is given by

$$\tau_1\, \mathrm{d}X_2 - \tau_2\, \mathrm{d}X_1 = 0. \tag{4-8}$$

The boundary is decomposed into three parts: the two horizontal lines $\Theta = \pi/2 \pm \pi/2$ and the cycloid where $\rho = \rho_m$. The traction-free boundary condition is satisfied for $\Theta = \pi/2 \pm \pi/2$ for all ρ and implies along the cycloid where $\rho = \rho_m$

$$\left(\frac{2b}{\alpha+1} - \frac{a_1}{\rho_m^{\alpha+1}}\right)\cos\Theta = 0. \tag{4-9}$$

This relation can be combined with (4-5); then

$$1 = \frac{2b}{\alpha+1}\left(\rho_m^{\alpha+1} + \frac{\alpha-1}{2}\right). \tag{4-10}$$

It can be noticed that the thickness H of the damaged zone is $H = ba\pi$.

For $\rho_m \to \infty$, the quantity b vanishes, the quasicrack tends to the classical crack, and the thickness H vanishes.

4B. ***Connection with release rate of energy.*** The strain energy for the critical shear R_m is given by

$$E(R_m) = \int_o^{R_m} \tau(t)\, \mathrm{d}t = \frac{1}{\mu_o}\frac{\tau_o^2}{\alpha+1}\left(\rho_m^{\alpha+1} + \frac{\alpha-1}{2}\right). \tag{4-11}$$

As a is a function of the equivalent loading K, the relation (4-10) determines the thickness of the damaged zone

$$\tfrac{1}{2}a\pi = \frac{H}{\alpha+1}\left(\rho_m^{\alpha+1} + \frac{\alpha-1}{2}\right) = \frac{1}{2}\frac{K^2}{\tau_o^2}. \tag{4-12}$$

The flux of the energy along the cycloid is given by

$$D_d = HE(R_m) = \pi a\frac{\tau_o^2}{2\mu_o} = \frac{K^2}{2\mu_o}. \tag{4-13}$$

This flux is exactly the energy release rate for the equivalent crack given by the condition of loading at infinity

$$\mathcal{G} = J = HE. \tag{4-14}$$

This emphasizes the fact that, in the presence of discontinuities of the displacement gradient along a curve Σ, the equivalent J-integral is obtained by the limit

$$\mathcal{G} = \lim_{\Gamma \to \Sigma} \int (En_1 - \boldsymbol{N\Theta} \cdot \boldsymbol{F} \cdot \boldsymbol{e}_1)\, \mathrm{d}s = \int_C (En_1 - \boldsymbol{N\Theta} \cdot \boldsymbol{F} \cdot \boldsymbol{e}_1)\, \mathrm{d}s \tag{4-15}$$

for all curve C containing the cycloid. The invariance of the integral can be proved as proposed in [Knowles and Sternberg 1972].

4C. ***Property of the solution for $\alpha \geq 0$.*** The balance equations for linear momentum are elliptic. If $\rho_o \geq \rho_1$, the volume bounded by the cycloid $(X(\rho_o, \Theta), Y(\rho_o, \Theta))$ contains the volume bounded by the cycloid $(X(\rho_1, \Theta), Y(\rho_1, \Theta))$. This is the case described by Neuber [1968].

In our approach, we have an additional equation that determines the thickness of the damaged zone with respect to the external loading. The equations of equilibrium are elliptic, and there are no discontinuities of the displacement gradient.

It can be noticed that we can use Rice's J-integral to evaluate the stress intensity factor K, taking into account the invariance of the J-type integral in hyperelasticity [Knowles and Sternberg 1972].

For $\rho_m = 1$, the results obtained by Bui and Ehrlacher are recovered, $b = 1$, and the solution is

$$X_1 = -\frac{1}{2} - \frac{1}{2\rho^2}\cos 2\Theta - \log \rho,$$
$$X_2 = -\frac{1}{2\rho^2}\sin 2\Theta + \left(\Theta - \frac{\pi}{2}\right),$$
$$W = -\left(\frac{1}{\rho} + \rho\right)\cos \Theta,$$

and the thickness of the damaged zone satisfies the relation

$$H = \pi a = \frac{K^2}{\tau_o^2}. \tag{4-16}$$

An estimation of the thickness for steel gives H of the order of $100\,\mu$m.

For $\alpha = 0$ and $\rho_m > 1$, the solution obtained by Bui [1980] is recovered.

It can be noticed that here the solution is obtained for nonlinear elastic behavior. This shows that Bui's solution is only a static solution. If we consider a propagation with constant velocity, the equation must be completely reformulated because in this case the inertia terms are not negligible with respect to the tangent modulus of the behavior.

Then the given relations are generalizations of these previous results to the case of hyperelastic brittle material.

4D. ***Property of the solution for $\alpha < 0$.*** In this case, the differential equation becomes hyperbolic for $\rho \geq 1$. The proposed potential U is the sum of two contributions: one independent of b and another one depending linearly on b. The first one corresponds exactly to the solution of Knowles and Sternberg for a classical crack in nonlinear elasticity.

But when ρ_m is finite, the main difficulty is to ensure the continuity of the displacement along the common boundary between the domains of ellipticity and hyperbolicity. It can be noticed that the limit

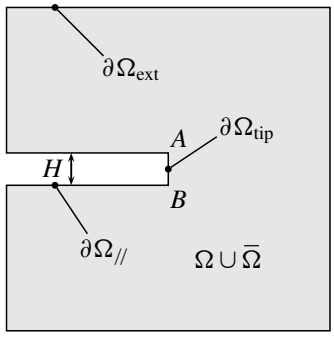

Figure 1. Meshed domain and boundary notations.

of the given potential when ρ_m tends to infinity is exactly the potential of Knowles and Sternberg because at the limit $b = 0$.

Another interesting limit is obtained for fixed value ρ_m and $\alpha \to -\infty$: the potential U tends toward the potential of the elastic brittle material, and the solution is the solution of Bui and Ehrlacher.

The general case will be discussed in a further paper; some new requirements about regularity are necessary to obtain a valuable solution.

5. Numerical approach

The problem of a quasicrack is now considered from a numerical point of view. The main difficulty is to determine the shape of the quasicrack with an optimization algorithm using a nonlinear solver. The goal of the numerical analysis is to determine numerically the traction-free boundary shape of the quasicrack and to exhibit the relationship between the thickness H, the material properties, and the stress intensity factor K of the equivalent crack.

To evaluate the ability of the proposed algorithm, we consider the constitutive law (2-12) with no loss of local ellipticity ($0 \leq \alpha \leq 1$).

Two main issues in the calculation have to be investigated: how to allow the free boundary to move and then how to adapt the stress intensity factor K during the calculation.

The meshed domain is a square with a quasicrack of a given thickness H as shown in Figure 1. The side of the square is ten times bigger than the quasicrack thickness. The boundary of the domain is decomposed into four parts: the outer boundary $\partial\Omega_{ext}$, the two crack lips $\partial\Omega_{//}$, and the nonmaterial boundary $\partial\Omega_{tip}$.

- The boundary $\partial\Omega_{ext}$ is supposed to be far enough from the equivalent crack tip to legitimately impose the loading determined in (4-5) and (2-13). At this stage, the stress intensity factor remains unknown.
- The boundary $\partial\Omega_{//}$ is a stress-free boundary; then $\boldsymbol{\sigma} \cdot n = 0$, where n is a normal vector to the material domain.
- The boundary $\partial\Omega_{tip}$ is used to close the meshed domain but has no physical meaning. The meshed domain is quite different than the material domain. The material boundary is represented by a curve Γ. In order to determine its position, a level set is used.

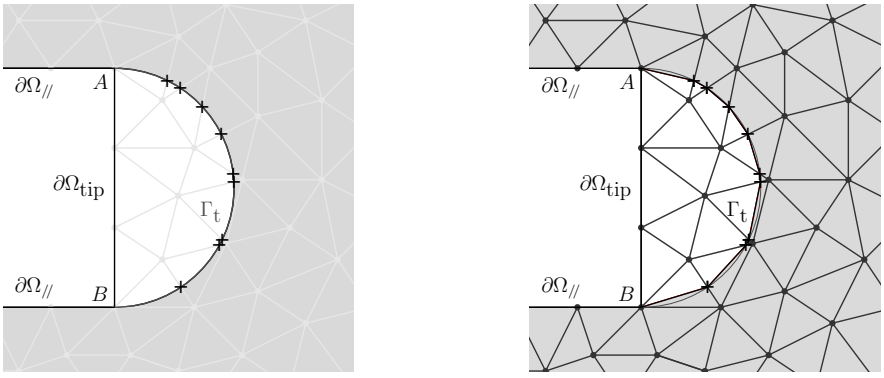

Figure 2. Material domain (gray) and damaged zone (white) are separated by the iso-zero of a level set Γ that is discretized as Γ_t. A coarse mesh is used here for a better understanding.

The level set Φ is chosen as the signed distance to Γ: Φ is positive in the material domain and negative outside. The level-set iso-zero ($\Phi(\boldsymbol{x}, t) = 0$) is the equation of Γ. Numerically, the level-set iso-zero matches Γ on the edges of the elements and approximates Γ inside the elements (see Figure 2) by Γ_t. Some elements are then cut by the material boundary, and the method "XFEM" is used to integrate only on the material domain [Moës et al. 1999; Daux et al. 2000].

It is important to note that the material domain will never contain $\partial\Omega_{\text{tip}}$. The level-set iso-zero is forced to contain the points A and B, so the material boundary Γ is the continuation of $\partial\Omega_{//}$ even if the curves are not forced to be tangent to A or B.

Global rigid solid motion is avoided by fixing a Dirichlet null condition on an arbitrary point of the material domain. The numerical solution is obtained by two complementary iterative processes: one to determine the equilibrium and another one to optimize the position of Γ.

During the computation of the equilibrium with a given position Γ_t, the amount of shear can exceed the critical value $R > R_m$. In that case, the same power law (2-12) is used for $R > R_m$. Knowing this state, an optimization process is then proposed to update the position of Γ_t with respect to the critical value R_m.

The shape optimization algorithm works as presented in Algorithm 1. To solve the mechanical non-linear problem, for a given Γ_t, an iterative algorithm is used (see Algorithm 2).

Shape optimization, convergence criterion, geometry evolution, and stress intensity factor updates are described in next subsections.

Initial shape Γ_o, solve
while traction-free boundary is not admissible with R_m **do**
  Compute hyperelasticity problem
  Update the level set
  Update the material domain and Γ_t
end while

Algorithm 1. Coarse description of shape optimization algorithm.

Resolution of a nonlinear elasticity problem
Determination of initial loading K and initial displacement w_o
while criterion$(\Delta K, \Delta w) >$ TOL **do**
  Compute w_n, Iter = Iter + 1,
if Iter > ITERMAX **then**
    Update K
    Compute a new correction w_{n+1}, Iter = 0
  end if
end while

Algorithm 2. Stress intensity factor update.

5A. ***Resolution of the hyperelastic boundary value problem.*** Applying a classical Newton–Raphson method to the hyperelasticity problem leads to instabilities for some values of α. The tangent operator associated with the constitutive law has the form

$$\begin{cases} \tau'(R) = \mu_0 & \text{for } R < R_o, \\ \tau'(R) = \mu_0 \alpha (R/R_o)^{\alpha-1} & \text{for } R > R_o. \end{cases} \tag{5-1}$$

This operator is discontinuous at $R = R_o$. For $R \geq R_o$, the value of the tangent operator can be so small that the stability of the algorithm is not ensured; the method is then relaxed by $u_{k+1} = u_k + \lambda \delta u_k$ with $\lambda \in [0, 1]$, and the tangent operator is replaced by a proportional value of it. So a line search method is used and defined as

$$\begin{cases} \tilde{\tau}'(R) = \mu_0 & \text{for } R < R_o, \\ \tilde{\tau}'(R) = \mu_0 (R/R_o)^{\alpha-1} & \text{for } R > R_o. \end{cases} \tag{5-2}$$

5B. ***Shape optimization.*** Once the hyperelasticity problem has been solved, the boundary Γ_t must be updated according to the condition $R = R_m$.

The evolution of Γ_t corresponds to updating the level-set iso-zero. The equation $\Phi(\boldsymbol{x}, t) = 0$ is the equation of a moving surface whose evolution is governed by its normal velocity a. The normal vector to Γ_t is given by $\nabla\Phi/\|\nabla\Phi\|$.

The velocity a is determined with respect to the condition $R = R_m$.

Firstly, strain field R is smoothed by solving a minimization problem whose variational formulation is,

$$\text{for all } \tilde{R}^*, \quad \int_\Omega \tilde{R}\tilde{R}^* \, \mathrm{d}\Omega = \int_\Omega R(w)\tilde{R}^* \, \mathrm{d}\Omega, \tag{5-3}$$

where $\tilde{R}$ and $\tilde{R}^*$ are continuous and w is the displacement field solution of the hyperelasticity problem.

Then the normal velocity $a = -k(\tilde{R} - R_{\text{ref}})/R_m$ is computed, $k > 0$. This velocity is smoothed over Γ_t by solving a diffusion problem in order to avoid instabilities in its evolution:

$$\text{for all } a^*, \quad \int_{\Gamma_t} \tilde{a}a^* \, \mathrm{d}\Gamma + \nu \int_{\Gamma_t} \nabla\tilde{a}\nabla a^* \, \mathrm{d}\Gamma = \int_{\Gamma_t} aa^* \, \mathrm{d}\Gamma, \tag{5-4}$$

where $\tilde{a}$ is the smoothed velocity field.

Shape optimization will be stopped when $\|a\|_\infty < a_{\text{tol}}$, where a_{tol} is about $\frac{1}{1000}$ of the geometry characteristic length.

5C. ***Geometry evolution and the updating of the level set.*** As Γ_t is updated by the normal velocity a determined previously, the level set has to be updated over the whole meshed domain. Two conditions must be satisfied. The updated level set must still be a signed distance function, and its iso-zero has to be located at a distance $\tilde{a}(s)$ of Γ_t, where s is a curvilinear abscissa of Γ_t. According to the definition of the normal velocity, the new position of Γ is then $\Gamma_{t+dt} = \Gamma_t + \tilde{a}(s)\boldsymbol{n}\,\mathrm{d}t$ with $\boldsymbol{n}$ the normal vector to Γ_t.

Let Φ be the level set and φ the shift for which we are looking. The solution must satisfy

$$\begin{cases} \|\nabla\Phi + \nabla\varphi\| = 1 & \text{in } \Omega, \\ \varphi = \tilde{a} & \text{on } \Gamma. \end{cases} \tag{5-5}$$

Moreover, Φ verifies $\|\nabla\Phi\| = 1$ and the system is equivalent to

$$\begin{cases} \Phi \cdot \varphi = 0 & \text{in } \Omega, \\ \varphi = \tilde{a} & \text{on } \Gamma_t. \end{cases} \tag{5-6}$$

This problem can be solved as an anisotropic diffusion problem:

$$\text{for all } \varphi^*, \quad \int_{\Gamma_t} \widetilde{\varphi}\varphi^*\,\mathrm{d}\Gamma + \mu \int_{\Omega\cup\overline{\Omega}} (\nabla\varphi\nabla\Phi)(\nabla\varphi^*\nabla\Phi)\,\mathrm{d}\Omega = \int_{\Gamma_t} \tilde{a}\varphi^*\,\mathrm{d}\Gamma, \tag{5-7}$$

where $\overline{\Omega}$ is the whole domain that contains the nonmaterial domain.

When φ is known, the level set Φ can be updated.

5D. ***The stress intensity factor update.*** The thickness H is fixed; to satisfy the condition $R = R_m$ over Γ_t, the stress intensity factor K must be updated during the iterative process of the hyperelastic problem resolution.

To have a good approximation of the stress intensity factor, three methods have been considered here. The most expensive one is to smooth the strain field over the whole material domain Ω as in (5-3) and to take its value at the points $\Gamma_t \cup \partial\Omega_{//}$. It is assumed that, at these points, R must be equal to R_m. The other methods consist of smoothing the strain field only over the free boundary Γ by solving a diffusion equation,

$$\text{for all } \tilde{R}^*, \quad \int_\Gamma (\tilde{R}\tilde{R}^* + L^2\nabla\tilde{R}\nabla\tilde{R}^*)\,\mathrm{d}\Gamma = \int_\Gamma R(w)\tilde{R}^*\,\mathrm{d}\Gamma, \tag{5-8}$$

where L^2 is the virtual diffusion coefficient. Then the mean value or the maximum one of the smoothed field is taken as a reference. The last option has been used to obtain the results presented here.

Stress intensity factor updates are expensive. They are not performed at each iteration of the nonlinear solver. However, a double convergence criterion is used: both displacement field and stress intensity factor tolerances have to be respected.

6. Some numerical results

Some tests are presented in order to estimate the performance of the method. The analytical solution of Section 4 is used to estimate the numerical accuracy of the algorithm.

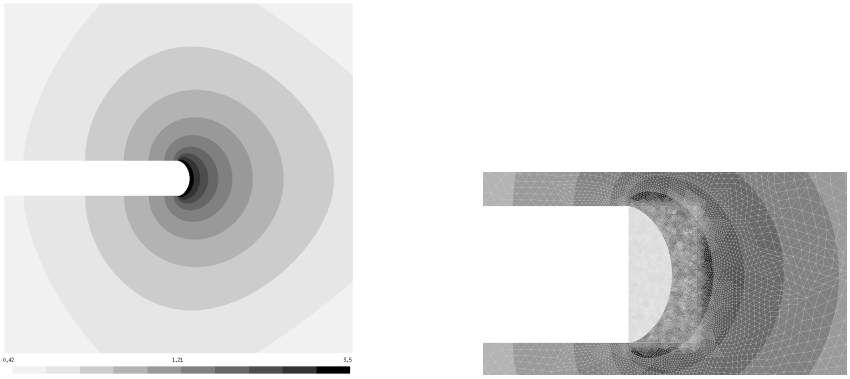

Figure 3. Smoothed strain $\tilde{R}$ (see (5-3)) at convergence: whole domain and detail over the quasicrack tip.

The algorithm has been applied to study the iso-R shapes and stress intensity factor values K for different values of ρ_m and α in the case of the power law (2-12). Finally, a bilinear brittle material is also studied.

6A. *Power law behavior with $\alpha > 0$.*

The shape of the traction-free boundary Γ_t. The criterion used to characterize the solution quality is the root mean square of the distance of each node of the boundary mesh to the analytical solution. This quantity is a length and represents the gap between the approximated and the analytical solutions. This value is compared to a characteristic length of the problem: the quasicrack thickness H.

Assume that the initial chosen shape is a semicircle. The initial gap is then 25% of characteristic length. At convergence, obtained after 88 iterations, the gap is reduced to 0.098%.

It is important to note that a precision of 0.002% is obtained at the first iteration when the computation is initialized with the analytical geometry.

Stress intensity factor. Analytical and numerical stress intensity factors K/R_o have been compared for different (R_m, α); the discrepancy is less than 1.2%. This shows that the thickness is very well evaluated.

The iso-R shape. The iso-R_o and iso-R_m are plotted at convergence in Figure 6. The relative gap is 0.005% for the curve R_m and 0.27% for the curve R_o.

The shape of the cycloids is well recovered.

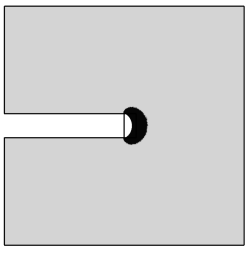

Figure 4. Elastic domain (gray) and hyperelastic one (black).

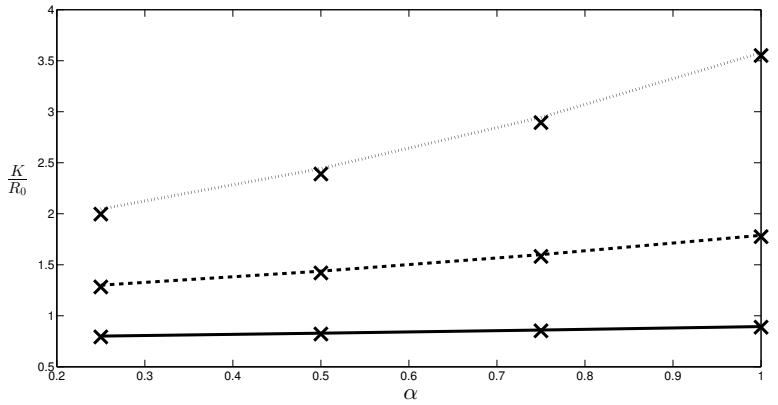

Figure 5. K/R_0 results for analytical and numerical calculations ($\times$) for the power law.

6B. ***The bilinear constitutive law.*** We consider now a bilinear constitutive law:

$$\begin{cases} R \le R_o, & \tau = \mu_o R, \\ R_o \le R \le R_m, & \tau = \tau_o + ((\tau_m - \tau_o)/(R_m - R_o))(R - R_o), \\ R_m \le R, & \tau = 0. \end{cases} \tag{6-1}$$

We note $\alpha = \tau_m/\tau_o$.

In Figure 7, the stress intensity factor K/R_o is plotted analytically using the equation connecting the J-integral and the thickness of the damaged zone:

$$J = \frac{K^2}{2\mu_o} = HE(R_m),$$
$$E(R_m) = \tfrac{1}{2}\tau_o R_o + \tau_o(R_m - R_o) + \tfrac{1}{2}(\tau_m - \tau_o)(R_m - R_o).$$

The numerical results are close to the analytical ones.

7. Conclusion

We have determined the shape of the damaged zone under antiplane shear conditions for hyperelastic brittle material. The analytical results are a generalization of preceding results obtained by Bui for brittle material. The thickness of the damaged zone is determined by the critical strain energy at rupture and the loading.

	$\rho_m = 2$		$\rho_m = 4$		$\rho_m = 8$	
α	analytical	numerical	analytical	numerical	analytical	numerical
0.25	0.8007	0.7931	1.3001	1.2825	2.0458	1.9964
0.50	0.8292	0.8216	1.4376	1.4199	2.4428	2.3896
0.75	0.8604	0.8528	1.5992	1.5821	2.9444	2.8941
1.00	0.8944	0.8878	1.7889	1.7756	3.5777	3.5513

Table 1. Analytical and numerical results, power law behavior.

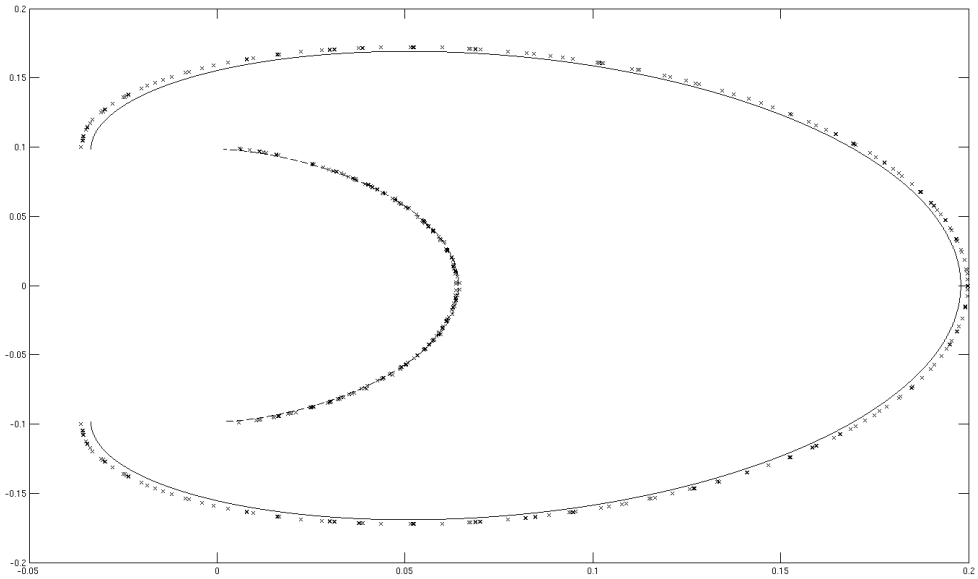

Figure 6. Comparison of the analytical (dashed line for R_o and solid for R_m) and numerical shapes ($\times$).

The case of power law stress-strain curve is discussed; it is used to evaluate the ability of a numerical optimization process applied to determine the damaged zone. An iterative scheme is proposed first to determine an equilibrium state and secondly to optimize the position of the boundary of the damage zone. The numerical results are close to the analytical results. The same algorithm is used for other constitutive laws.

The approach must be extended to other cases of loading especially mode I and more general local behavior.

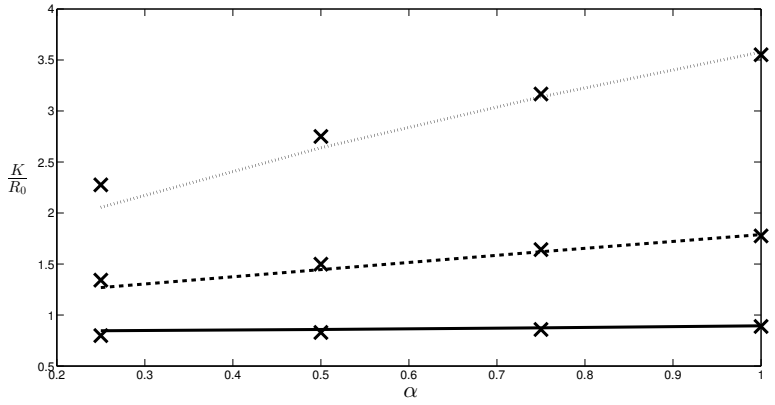

Figure 7. K/R_0 results for analytical and numerical calculations for bilinear behavior.

	$\rho_m = 2$		$\rho_m = 4$		$\rho_m = 8$	
α	analytical	numerical	analytical	numerical	analytical	numerical
0.25	0.8462	0.7986	1.2692	1.3420	2.0556	2.2759
0.50	0.8585	0.8291	1.4454	1.4986	2.6398	2.7504
0.75	0.8747	0.8584	1.6202	1.6413	3.1381	3.1667
1.00	0.8944	0.8878	1.7889	1.7756	3.5777	3.5513

Table 2. Analytical and numerical comparison, bilinear material.

The proposed method based on level-set and XFEM modelization should be extended also to the damage transition to rupture modeled by thick level set [Moës et al. 2011], where the damage d evolves from 0 to 1 in a layer of finite thickness l_c. Two particular level-set values must be introduced: one $\Phi(\boldsymbol{x}, t) = 0$ to described the boundary where $d = 0^+$, the other $\Phi(\boldsymbol{x}, t) = l_c$ where $d = 1$. The case presented here is $l_c = 0$. For $l_c \neq 0$, this type of approach addresses the existence or not of a quasicrack for constitutive behavior with smooth transition between damage to rupture.

References

[Bui 1980] H. D. Bui, "Solution explicite d'un problème de frontière libre en élastoplasticité avec endommagement", *C. R. Acad. Sci. Paris B Sci. Phys.* **290** (1980), 345–348.

[Bui and Ehrlacher 1980] H. D. Bui and A. Ehrlacher, "Propagation dynamique d'une zone endommagée dans un solide élastique-fragile en mode III et en régime permanent", *C. R. Acad. Sci. Paris B Sci. Phys.* **290** (1980), 273–276.

[Daux et al. 2000] C. Daux, N. Moës, J. Dolbow, N. Sukumar, and T. Belytschko, "Arbitrary branched and intersecting cracks with the extended finite element method", *Int. J. Numer. Methods Eng.* **48**:12 (2000), 1741–1760.

[Knowles and Sternberg 1972] J. K. Knowles and E. Sternberg, "On a class of conservation laws in linearized and finite elastostatics", *Arch. Ration. Mech. Anal.* **44**:3 (1972), 187–211.

[Knowles and Sternberg 1980] J. K. Knowles and E. Sternberg, "Discontinuous deformation gradients near the tip of a crack in finite anti-plane shear: an example", *J. Elasticity* **10**:1 (1980), 81–110.

[Knowles and Sternberg 1981] J. K. Knowles and E. Sternberg, "Antiplane shear fields with discontinuous deformation gradients near the tip of a crack in finite elastostatics", *J. Elasticity* **11**:2 (1981), 129–164.

[Moës et al. 1999] N. Moës, J. Dolbow, and T. Belytschko, "A finite element method for crack growth without remeshing", *Int. J. Numer. Methods Eng.* **46**:1 (1999), 131–150.

[Moës et al. 2011] N. Moës, C. Stolz, P.-E. Bernard, and N. Chevaugeon, "A level set based model for damage growth: the thick level set approach", *Int. J. Numer. Methods Eng.* **86**:3 (2011), 358–380.

[Neuber 1968] H. Neuber, "A physically nonlinear notch and crack model", *J. Mech. Phys. Solids* **16**:4 (1968), 289–294.

[Stolz 2010] C. Stolz, "Closed form solution for the finite anti-plane shear field for a class of incompressible brittle solids", *C. R. Mécanique* **338**:12 (2010), 663–669.

Received 7 Mar 2014. Revised 6 Feb 2015. Accepted 2 Mar 2015.

CLAUDE STOLZ: claude.stolz@ec-nantes.fr
Génie civil et Mécanique, UMR CNRS 6183, 1 rue de la Noë, 44321 Nantes, France

and

IMSIA EDF UMR CNRS 9219, 1 avenue Charles de Gaulle, 92141 Clamart, France

ANDRES PARRILLA GOMEZ: andres.parrilla-gomez@ec-nantes.fr
Génie civil et Mécanique, UMR CNRS 6183, 1 rue de la Noë, 44321 Nantes, France

JOURNAL OF MECHANICS OF MATERIALS AND STRUCTURES

msp.org/jomms

Founded by Charles R. Steele and Marie-Louise Steele

See msp.org/jomms for submission guidelines.

JoMMS (ISSN 1559-3959) at Mathematical Sciences Publishers, 798 Evans Hall #6840, c/o University of California, Berkeley, CA 94720-3840, is published in 10 issues a year. The subscription price for 2015 is US $565/year for the electronic version, and $725/year (+$60, if shipping outside the US) for print and electronic. Subscriptions, requests for back issues, and changes of address should be sent to MSP.

JoMMS peer-review and production is managed by EditFLOW® from Mathematical Sciences Publishers.

PUBLISHED BY

mathematical sciences publishers

nonprofit scientific publishing

http://msp.org/

Journal of Mechanics of Materials and Structures

Volume 10, No. 3 May 2015

Special issue

In Memoriam: Huy Duong Bui

Huy Duong Bui — JEAN SALENÇON and ANDRÉ ZAOUI 207

The reciprocity likelihood maximization: a variational approach of the reciprocity gap method — STÉPHANE ANDRIEUX 219

Stability of discrete topological defects in graphene — MARIA PILAR ARIZA and JUAN PEDRO MENDEZ 239

A note on wear of elastic sliding parts with varying contact area — MICHELE CIAVARELLA and NICOLA MENGA 255

Fracture development on a weak interface near a wedge — ALEXANDER N. GALYBIN, ROBERT V. GOLDSTEIN and KONSTANTIN B. USTINOV 265

Edge flutter of long beams under follower loads — EMMANUEL DE LANGRE and OLIVIER DOARÉ 283

On the strong influence of imperfections upon the quick deviation of a mode I+III crack from coplanarity — JEAN-BAPTISTE LEBLOND and VÉRONIQUE LAZARUS 299

Interaction between a circular inclusion and a circular void under plane strain conditions — VLADO A. LUBARDA 317

Dynamic conservation integrals as dissipative mechanisms in the evolution of inhomogeneities — XANTHIPPI MARKENSCOFF and SHAILENDRA PAL VEER SINGH 331

Integral equations for 2D and 3D problems of the sliding interface crack between elastic and rigid bodies — ABDELBACET OUESLATI 355

Asymptotic stress field in the vicinity of a mixed-mode crack under plane stress conditions for a power-law hardening material — LARISA V. STEPANOVA and EKATERINA M. YAKOVLEVA 367

Antiplane shear field for a class of hyperelastic incompressible brittle material: Analytical and numerical approaches — CLAUDE STOLZ and ANDRES PARRILLA GOMEZ 395

Some applications of optimal control to inverse problems in elastoplasticity — CLAUDE STOLZ 411

Harmonic shapes in isotropic laminated plates — XU WANG and PETER SCHIAVONE 433

1559-3959(2015)10:3;1-A